Fatigue crack initiation site and propagation paths in high-cycle fatigue of magnesium alloy AZ31

Nakai, Yoshikazu
Saka, Masahiko
Yoshida, Hayata
Asayama, Kaito
Kikuchi, Shoich

(Citation)
International Journal of Fatigue,123:248-254

(Issue Date)
2019-06

(Resource Type)
journal article

(Version)
Accepted Manuscript

(URL)
https://hdl.handle.net/20.500.14094/90005902

Title page

Fatigue Crack Initiation Site and Propagation Paths in High-cycle Fatigue of Magnesium Alloy AZ31

Yoshikazu NAKAI[a,*], Masahiko SAKA[a], Hayata YOSHIDA[a], Kaito ASAYAMA[a], and Shoich KIKUCHI[b]

[a]Department of Mechanical Engineering, Kobe University

1-1, Rokkodai, Nada, Kobe 657-8501, Japan

[b]Department of Mechanical Engineering, Shizuoka University

3-5-1, Johoku, Naka, Hamamatsu 432-8561, Japan

*: Corresponding author, Phone: +81-78-803-6128, Facsimile: +81-78-803-6155

E-mail: nakai@mech.kobe-u.ac.jp

Abstract

Plane bending fatigue tests were conducted under stress ratios of -1, -0.1, 0.1, and 0.5 at room temperature in a laboratory atmosphere to elucidate the fatigue crack initiation mechanism of an extruded AZ31 magnesium alloy. The fatigue life can be expressed as a unique function of the equivalent stress amplitude based on Smith–Watson–Topper theory independent of the stress ratio, and the dependence of the fatigue limit on the mean stress can be expressed by Morrow's equation, both of which were proposed for conventional metals without twinning. In addition, the specimen surface was observed by optical microscopy and scanning electron microscopy (SEM), and the surface near the crack initiation site was analyzed by electron backscatter diffraction (EBSD) analysis to discuss the fatigue crack initiation mechanism. On the basis of the results of EBSD analysis, it is concluded that the existence of large grain with large Schmid factor of the basal slip system is essential for crack initiation, and the crack initiation mechanism is based on irreversible slipping and unrelated to twinning under the alternating stress condition (R=-1).

Keywords

Fatigue; Crack initiation; Twinning; Stress ratio; Magnesium alloy; EBSD analysis.

1. Introduction

To reduce global warming problem, the improvement of energy-saving systems is required, particularly for transportation, and the utilization of high-specific-strength materials is one of the most promising approaches for accomplishing such improvement. Since magnesium alloys have the highest specific strength among the engineering metallic materials, they have received considerable attention. However, it is necessary to guarantee their long-term strength by clarifying their fatigue fracture mechanisms before these alloys can be employed for structural use.

Because the slip system is limited for magnesium alloys with a hexagonal close-packed (hcp) crystal structure, twinning is an important mechanism of plastic deformation, especially under the compression stress. In the high-cycle fatigue of metallic materials, however, plastic deformation only occurs in part of the grains, and slip bands cannot be observed in all the grains [1-3]. Thus, the twinning may not be essential for crack initiation. Regardless of the involvement of twinning, fatigue cracks are considered to initiate from grains where the Schmid factor of the basal plane is sufficiently high for slipping to occur. Shiozawa et al. found that the fatigue crack initiation mechanism changed from the twin-induced failure mode at high stress amplitudes to the slip-induced failure mode at low stress amplitudes [4]. Therefore, fatigue cracks are usually initiated from twin boundaries in polycrystalline magnesium alloys without defects or inclusions in the low-cycle fatigue regime [4-6], where all grains should be deformed plastically. However, it is unclear whether twinning is involved in crack initiation in the high-cycle fatigue regime [4,6-13]. Shiozawa et al. also studied the effect of the stress ratio on the fatigue properties of an extruded

AZ80 alloy [4] and concluded that a clear fatigue limit existed in the pulsating fatigue test (R=0), while stepwise S–N curves with two knees were observed for fully reversed cyclic loading (R=-1). Yang et al. reported that the S–N curve of an extruded AZ31 alloy with R=-1 appeared to monotonically decrease in the very high-cycle fatigue regime, and fatigue cracks were observed along twin bands [9]. Tokaji et al. [14] and Ochi et al. [15] reported for an extruded AZ31 alloy that a clear fatigue limit existed and stepwise S–N curves with two knees were not observed.

In the present study, experiments were conducted to determine whether twinning is involved in the fatigue crack initiation mechanism and conventional fatigue limit are exist for a magnesium alloy in the high-cycle fatigue regime.

2. Material and experimental procedures

The material used in the present study was an extruded AZ31 magnesium alloy with a composition (in mass %) of 2.7Al, 0.79Zn, 0.44Mn, 0.0012Fe, 0.009Ni, 0.011Cu, 0.004Si, and balance Mg. Inverse pole figure (IPF) maps of the alloy obtained by electron backscatter diffraction (EBSD) analysis is shown in Figure 1, which shows the crystallographic orientations of grains relative to the normal to each cross section. The material has a texture in which the c-axis of the crystals is normal to the specimen surface. The average grain size of the alloy is 52 μm and the tensile and compressive yield strengths are 286 and 79 MPa, respectively.

The geometry and dimensions of the fatigue test specimens are shown in Figure 2. The specimens were cut by wire electric discharge machining from an extruded plate so that the

longitudinal direction of the specimen coincided with the direction of extrusion. The stress concentration factor of the specimen at the shallow notch, K_t, was 1.04 under plane bending in which the specimen received the maximum stress at the plate surface [16].

A computer-controlled electrodynamic testing machine was used for the fatigue experiments. Since the machine generated an axial force, an in-plane cyclic bending moment was applied to the specimen through a loading device with an arm length of 20 mm. The tests were conducted with the stress ratio R ranging from -1 to 0.5 (where R is the ratio of the minimum to maximum bending moment during one fatigue loading cycle) with a frequency of 30 Hz.

3. Experimental results

3.1 Fatigue life and fatigue limit

The S–N curve of a smooth specimen is shown in Figure 3 (a). According to the present results, a clear fatigue limit existed in the case of R=-1, and stepwise S–N curves with two knees were not observed. This is consistent with the results obtained by Tokaji et al. [16] and Ochi et al. [17].

Figure 3 (b) shows the number of cycles to failure, N_f, as a function of the equivalent stress amplitude defined by Smith et al. [18], where $\sigma_{max}=2\sigma_a/(1-R)$. Although the minimum stress exceeded the twinning stress under compression in the case of fully reversed cyclic loading (R=-1), and twinning must not have occurred for $R\geq$-0.1 tests, the relation shown in Figure 3 (b) is similar to that for conventional alloys without twinning. This indicates that the fatigue failure was not

affected by twinning.

To estimate the effect of the mean stress on the fatigue limit, several relationships have been proposed [19]. These relations are shown in Figure 4, together with the experimental results in this study, where σ_{w0} is the fatigue limit for σ_m=0 (R=-1), σ_{UTS} is the ultimate tensile strength, and σ_T is the true fracture stress. Although Shiozawa et al. reported that their experimental results fit the modified Goodman's relationship [20], the present results best fit the Morrow equation, which was proposed for alloys without twinning.

Figure 5 shows an example of crack initiation and propagation behaviors, where arrows indicate crack tips. A crack was first found around the corner of the specimen at N=3×10^3 cycles, as shown in Figure 5(b) observed at high magnification. At the early stage of crack propagation, flexions of the crack path were observed, and it is not clear whether twinning deformation was involved in the crack initiation from these images. Figure 6 shows the crack length as a function of the number of cycles normalized by that to the final failure, N_f. The normalized crack initiation life was almost the same regardless of the stress ratio and stress amplitude, indicating that twin deformation is not involved in the fatigue crack initiation mechanism because twinning occurs in fatigue tests under R=-1 but does not occur under R=0.1.

Although the crack growth curves differ among the three conditions in Figure 6, the crack growth rate da/dN can be expressed as a function of the stress intensity range ΔK as shown in Figure 7, where the stress intensity factor was calculated using the formula proposed by Newman and Raju [21], and only the positive part of the stress range is used for R=-1 in the calculation of

the stress intensity factor range. The growth rate of the small crack, da/dN, for R=0.1 was almost the same as that of the long crack at the same stress ratio, which was obtained from the C(T) specimen with a width of 24 mm and a thickness of 2 mm, and no short crack effect was observed [22]. An almost unique relationship is obtained for the results of R=-1, and the relationship is almost indepent of the stress ratio, as reported by Nakai et al. for long cracks in mild steel in Paris–Erdogan Law region [23].

3.2 Fractography

Figure 8 shows fractographs of fatigued specimens under R=-1 and 0.1, where stripe patterns with a stripe width approximately equal to the grain size can be observed, with a similar morphology of the fracture surface for each stress ratio. Shiozawa et al. speculated that the stripe pattern is related to twinning without providing direct evidence [24]. A similar stripe pattern was observed in the fracture surface of low-carbon steel as a result of the pencil glide slip of bcc materials [23, 25]. On the other hand, Sakai et al. observed a similar stripe morphology for the fracture surface of a magnesium alloy but found no twinning by EBSD analysis [26]. Thus, the stripe patterns indicate the occurrence of slip.

As shown in Figure 9, a shallow crack was initiated near the corner of the specimen, which corresponded to the crack profiles shown in Figure 5, and the morphology of the crack initiation site was flat without a stripe pattern, which was different from that in the crack propagation area.

4. Discussion

Although several papers have reported on the effect of twinning on crack initiation in magnesium alloys, universally accepted conclusions have not yet been obtained. Not only is there speculation based on the geometry without the orientation analysis of grains, some ambiguity also still remains in EBSD, although it can be used for the rigorous justification of twinning.

The EBSD analysis was conducted for a specimen fatigued under R=-1 to clarify whether twin deformation was involved in fatigue crack initiation. Figure 10 shows IPF maps obtained by the EBSD analysis of a specimen that failed at a stress amplitude of 140 MPa, combined with the crack profiles obtained from Figure 5, which are indicated by white lines. It is clear from Figure 10 (a) that no twin deformation occurred at the crack initiation site.

To clarify the crack profiles to examine successive crack profiles, tensile stress was applied to a specimen in order to open cracks for observation by optical microscopy. For the specimen shown in Figure 10, the EBSD analysis was conducted after the failure of the specimen. Before the EBSD analysis, the surface of the specimen was mechanically polished to remove the surface oxidation layer, which is required for the EBSD analysis of magnesium alloys. Even if twinning occurs under compression stress, detwinning occur following tensile loading [26-28]. However, tensile stress does not apply to cracked grains and detwinning does not occur after crack initiation. It is possible that mechanical polishing also affects the twinning and detwinning behavior.

To confirm the validity of this procedure, the fatigue tests were interrupted immediately after crack initiation, and compression stress was applied to the specimen. To remove the surface

oxidation layer, cross-sectional polishing was conducted while minimizing the damage by performing Ar ion milling before the EBSD analysis instead of mechanical polishing. The results for the high-cycle fatigue regime are shown in Figure 11, where white lines indicate the crack profiles observed at each number of cycles. No twinned crystals were observed at the crack initiation or propagation sites, indicating that twinning is not involved in the crack initiation or the early stage of crack propagation in the case of high-cycle fatigue. It also indicates that the stripe patterns on the fracture surface are not the result of twinning.

Since the crack had already penetrated several grains at the first observation (Figure 11 (a) N=1.0×10^3 cycles), the initiation site was difficult to identify. Then, careful observation was conducted on a different specimen at a lower stress amplitude, σ_a, of 120 MPa. It was found that two cracks were formed at a nearby site, as shown in Figure 12 (b) and (c), which merged to form a single crack between 1.8×10^4 and 2.0×10^4 cycles, as indicated in Figure 12(e) and Figure 13. The EBSD analysis was conducted at the site indicated in Figure 12 (f), and the results are shown in Figures 14 and 15, where the former shows the orientations of grains and crack profiles at each number of cycles obtained from Figure 12, and the latter indicates the Schmid factor of the basal slip system. Table 1 shows the size and Schmid factor of the basal slip system for grains specified in Figure 15. These indicate that Grains I and II were large and had large Schmid factor of the basal slip system. Also, those grains were adjacent to small grains. In these figures, it is not clear whether cracks initiated from large grains adjacent to small grains, or small grains adjacent to large grains, however the existence of large grains with large Schmid factor is considered to be

essential for crack initiation because cracks were propagated into large grains just after the initiation.

The above findings strongly indicate that fatigue cracks are initiated as a result of irreversible slipping by dislocation motion and that twinning is not involved in the high-cycle fatigue crack initiation mechanism, for which several mechanisms have been proposed. Defects and inclusions may not be involved in fatigue crack initiation because of the recent development of fabrication techniques of the magnesium alloys. The effect of the texture and/or grain size may explain the difference of the crack initiation mechanism although this cannot be concluded without careful EBSD analysis.

5. Conclusions

Plane bending fatigue tests were conducted at room temperature in a laboratory atmosphere under several stress ratios to examine whether the twinning is involved in the fatigue crack initiation of an extruded AZ31 magnesium alloy. The following results were obtained.

(1) The fatigue life can be expressed as a unique function of the equivalent stress amplitude based on Smith–Watson–Topper theory independent of the mean stress, and the dependence of the fatigue limit on the mean stress can be expressed by Morrow's equation, both of which were proposed for conventional metals without twinning.

(2) The fatigue crack initiation life normalized by the number of cycles to failure under an alternating stress condition (R=-1), where the minimum stress exceeded the twinning stress under compression, is almost identical to that under pulsating stress (R>0), indicating that twinning is not related to the

fatigue crack initiation mechanism.

(3) Careful observation of a specimen fatigued under the alternating stress by optical microscopy and EBSD analysis revealed that no twinning occurred at the crack initiation site. The existence of large grains with large Schmid factor of the basal slip system is essential for crack initiation. Thus, twinning is not involved in the fatigue crack initiation mechanism of the high-cycle fatigue regime of the extruded AZ31 magnesium alloy.

Acknowledgement

Support of this work through a Grant-in-Aid for Scientific Research (C) from Japan Society for the Promotion of Science under proposal number 18K03837 (Head investigator: Professor Y. Nakai, Kobe University) is gratefully acknowledged. The authors would like to thank Dr. Yuki Nakamura (National Institute of Technology, Toyota College) for their experimental support.

References

[1] Tanaka K, Nakai Y, Maekawa O. Microscopic study on fatigue crack initiation and early propagation in smooth specimen of low carbon steel. J. Soc. Materials, Japan 1982;31:376-82.

[2] Nakai Y, Fukuhara S, Ohnishi K. Observation of fatigue damage in structural steel by scanning atomic-force microscopy. Int. J. Fatigue 1997;19:S223-S36.

[3] Nakai Y, Kusukawa T, Hayashi N. Scanning atomic-force microscopy on initiation and growth behavior of fatigue slip-bands in α-brass. Fatigue and Fracture Mechanics: 32nd Volume, ASTM STP 1406, R. Chona, Ed., American Society for Testing and Materials, West Conshohoken, PA, 2002:122-35.

[4] Shiozawa K, Kashiwagi T, Murai T, Takahashi T. Gigacycle fatigue behavior and fractography of extruded AZ80 magnesium alloy. Trans. Japanese Soc. Mech. Eng. A. 2009;75:733-41.

[5] Begum S, Chen DL, Xu S, Luo AA. Effect of strain ratio and strain rate on low cycle fatigue behavior of AZ31 wrought magnesium alloy. Mat. Sci. Eng. A 2009;517:334-43.

[6] Matsuzuki M, Horibe S. Analysis of fatigue damage process in magnesium alloy AZ31. Mat. Sci. Eng. A 2009;504:169-74.

[7] Nan ZY, Ishihara S, Goshima T, Nakanishi R. Scanning probe microscope observations of fatigue process in magnesium alloy AZ31 near the fatigue limit. Scripta Meter. 2004;50:429-34.

[8] Kamakura M, Tokaji K, Ishizumi Y, Hasegawa N. Fatigue behavior and fracture mechanism of an extruded AZ61 magnesium alloy. J. Soc. Mat. Sci, Japan 2004;53:1371-7.

[9] Yang F, Yin SM, Li SX, Zhang ZF. Crack initiation mechanism of extruded AZ31 magnesium alloy

in the very high cycle fatigue regime. Mat. Sci. Eng. A 2008;491:131-6.

[10] Uematsu Y, Sugie T. Effect of grain orientation on small fatigue crack growth behavior in magnesium alloy AZ31 rolled plate. Trans. Japanese Soc. Mech. Eng. A 2010;76:311-6.

[11] Nascimento L, Bohlen SYJ, Fuskova L, Letzig D, Kainer KU. High cycle fatigue behavior of magnesium alloys. Proc. Eng. 2010;2:743-50.

[12] King A, Ludwig W, Herbig M, Buffiére JY, Khan AA. Three-dimensional in situ observations of short fatigue crack growth in magnesium. Acta Mater. 2011;59:6761-71.

[13] Uematsu Y, Kakiuchi T, Tamada K, Kimia Y. EBSD analysis of fatigue crack initiation behavior in coarse-grained AZ31 magnesium alloy. Int. J. Fatigue 2016;84:1-8.

[14] Tokaji K, Kamakura M, Ishizumi Y, Hasegawa N. Fatigue behavior and fracture mechanism of a rolled AZ31 magnesium alloy. Int. J. Fatigue 2004;26:1217-24.

[15] Ochi Y, Masaki K, Hirasawa T, Wu X, Matsumura T, Takigawa Y, Higashi K. High cycle fatigue property and micro crack propagation behavior in extruded AZ31 magnesium alloys. Mater. Trans. 2006;47:989-94.

[16] Neuber H. Kerbspannungslehre, Zweite Auflage. Springer-Verlag, Berlin/Göttingen/ Heiderberg, 1958:84.

[17] JSMS Committee on Fatigue of Materials and JSMS Committee on Reliability Engineering, “Standard Evaluation Method of Fatigue Reliability for Metallic Materials – Standard Regression Method of S-N Curves – [JSMS-SD-6-08], The Society of Materials Science, Japan; 2008.

[18] Smith KN, Watson P, Topper H. A stress function for the fatigue of metals. J. Mat. 1970;5:767-78.

[19] Ince A, Glinka G. A modification of Morrow and Smith–Watson–Topper mean stress correction models. Fatigue Fract. Eng. Mat. Struct. 2011;34:854-67.

[20] Shiozawa K, Ikeda A, Fukumori T. Effect of stress ratio and loading mode on high cycle fatigue performances of extruded magnesium alloys, Trans. Japanese Soc. Mech. Eng. A. 2013;79;1366-1381.

[21] Newman Jr. JC, Raju S. An empirical stress-intensity factor equation for the surface crack. Eng. Fract. Mech. 1981;15:185-92.

[22] Tanaka K, Hojo M, Nakai Y. Fatigue crack initiation and early propagation in 3% silicon iron, fatigue mechanisms: Advances in quantitative measurement of physical damage. J. Lankford, D. L. Davidson, W. L. Morris, and R. P. Wei, eds., ASTM STP 1983;811:207-32.

[23] Nakai Y, Tanaka K, Nakanishi T. The effects of stress ratio and grain size on near-threshold fatigue crack propagation in low-carbon steel. Eng. Fract. Mech. 1981;15:291-302.

[24] Otsuka A, Mori K, Kawamura T. A fractographic investigation of fatigue crack initiation and initial growth in mild steel. J. Soc. Materials, Japan 1978;27:49-53.

[25] Shiozawa K, Nagai M, Murai T, Takahashi T. Low cycle fatigue behavior of extruded AZ80 magnesium alloys. J. Soc. Materials, Japan 2009;58:235-42.

[26] Sakai T, Kikuchi S, Nakamura Y, Ninomiya N. A study on very high cycle fatigue properties of low flammability magnesium alloy in rotating bending and axial loading. Appl. Mech. Mater. 2015;782:27-41.

[27] Wu L, Jain A, Brown DW, Stoica GM, Agnew SR, Clausen B, Fielden DE, Liaw PK.

Twinning-detwinning behavior during the strain-controlled low-cycle fatigue testing of a wrought magnesium alloy, ZK60A. Acta Mater. 2008;56:688-95.

[28] Wu L, Agnew SR, Brown DW, Stoica GW, Clausen B, Jain A, Fielden DE, Liaw PK. Internal stress relaxation and load redistribution during the twinning-detwinning-dominated cyclic deformation of a wrought magnesium alloy, ZK60A. Acta Mater. 2008;56:3699-707.

[29] Nakai Y, Shiozawa D, Kikuchi S. In-situ observation of formulation of twinning for magnesium alloy by diffraction contrast tomography. http://support.spring8.or.jp/Report_JSR/PDF_JSR_28B/2016B1627.pdf 2017.

List of Table and Figures

Figure 10. Inverse pole figure (IPF) map obtained by EBSD analysis failed at stress amplitude of 140 MPa under the stress ratio, R, of -1, at N= (a) 3.0×10^3, (b) 6.0×10^3, (c) 8.0×10^3, (d) 1.0×10^4, (e) 1.2×10^4, (f) 1.4×10^4 cycles, respectively, where white lines indicate the crack profile at the number of cycles.

Figure 11. Inverse pole figure (IPF) map obtained by EBSD analysis of specimen fatigued at the stress amplitude of 140 MPa under the stress ratio, R, of -1, at N= (a) 1.0×10^3, (b) 2.0×10^3, (c) 3.0×10^3, (d) 4.0×10^3 cycles, respectively, where white lines indicate the crack profile at the number of cycles.

Figure 12. Crack initiation and propagation behaviors for a specimen fatigued under σ_a=120 MPa, R = -1, at N= (a) 0, (b) 2.0×10^3, (c) 4.0×10^3, (d) 1.2×10^4, (e) 2.0×10^4, (f) 6.0×10^4 cycles, respectively.

Figure 13. Crack growth curves.

Figure 14. Orientation of grains around crack initiation site under σ_a=120 MPa, R = -1, at N= (a) 2.0×10^3, (b) 4.0×10^3, (c) 1.2×10^4, (d) 2.0×10^4 cycles, respectively, where white lines indicate the crack profile at the number of cycles.

Figure 15. Schmid factor of basal slip system for grains around crack initiation site and crack profiles under σ_a=120 MPa, R = -1, at N= (a) 2.0×10^3, (b) 4.0×10^3, (c) 1.2×10^4, (d) 2.0×10^4 cycles, respectively, where black lines indicate the crack profile at the number of cycles.

Table 1. Size and Schmid factor of basal slip system for grains around crack initiation site.

Grain	Grain size (μm)	Schmid factor
I	107	0.34
II	94	0.50
III	19	0.43
IV	54	0.45

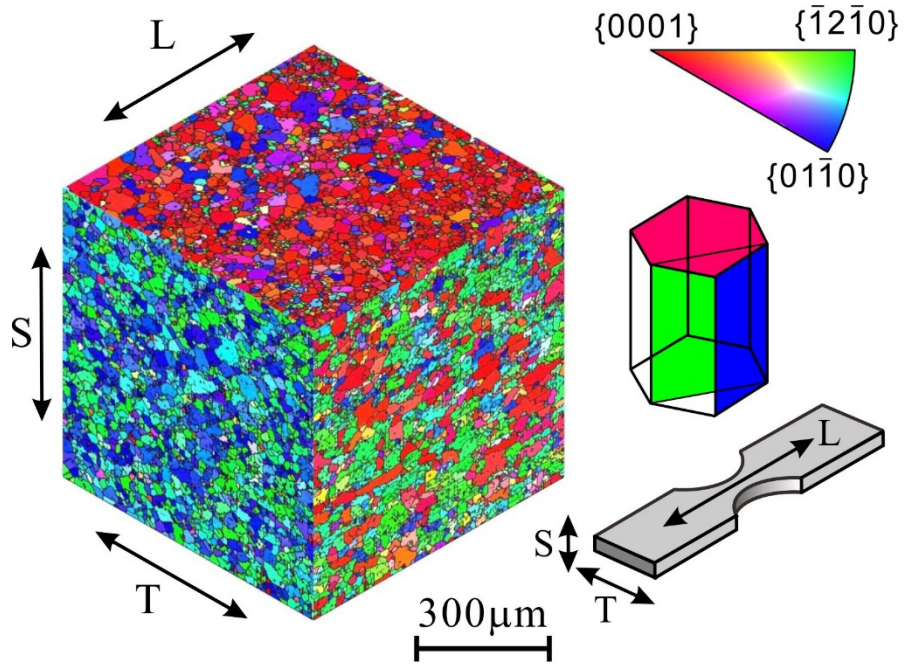

Figure 1. Inverse pole figure (IPF) map obtained by EBSD analysis for AZ31 alloy indicating the crystallograpic orientation to the normal to each plane.

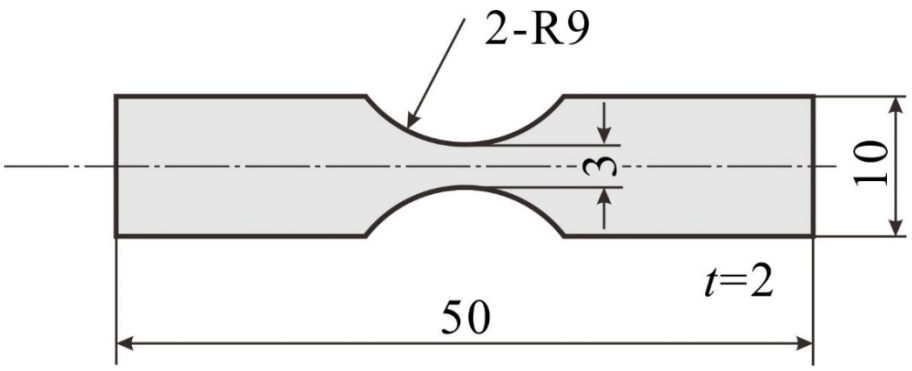

Figure 2. Shape and dimensions of specimen.

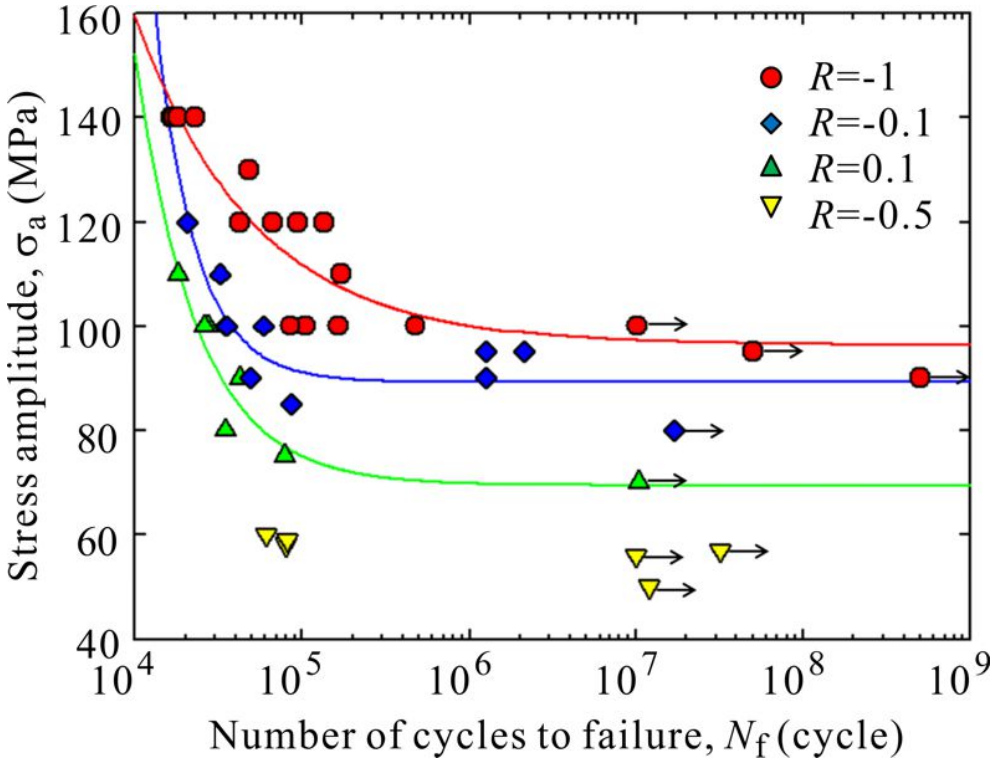

(a) Stress amplitude,σ_a, vs. number of cycles to failure, N_f.

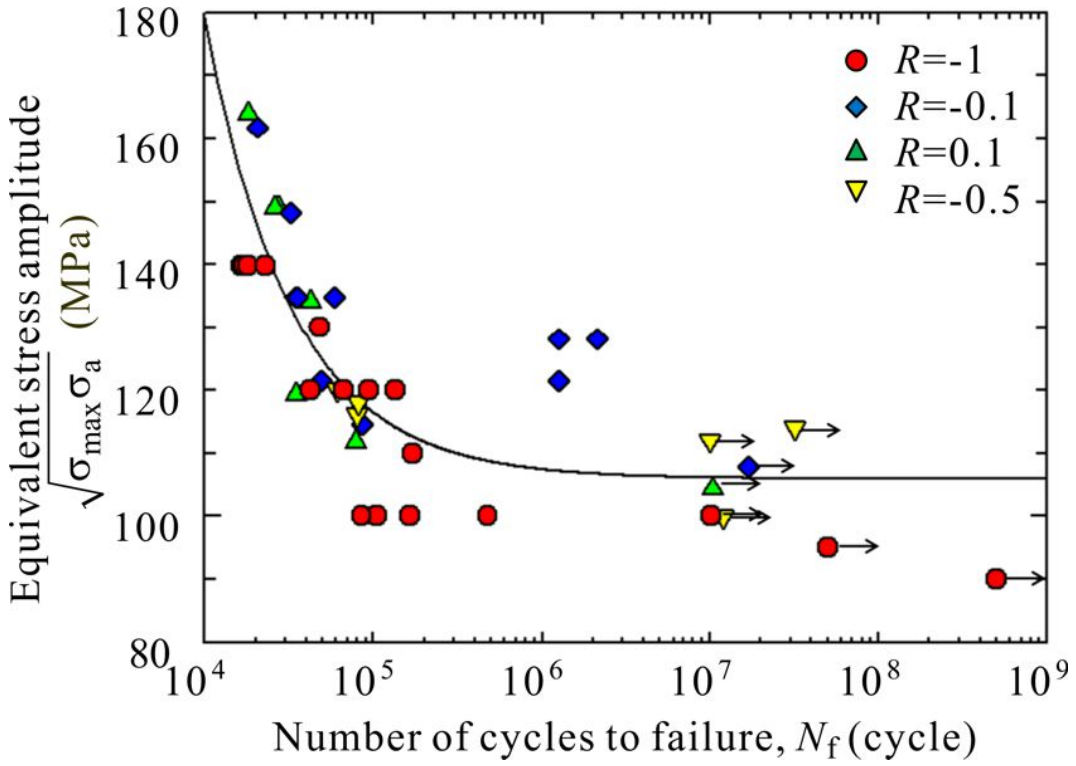

(b) Equivalent stress amplitude, $\sqrt{\sigma_{max}\sigma_a}$, vs. number of cycles to failure, N_f.

Figure 3. *S–N* curves, where regression curves were calculated using standard regression method of *S–N* curves proposed by the Society of Materials Science, Japan [17].

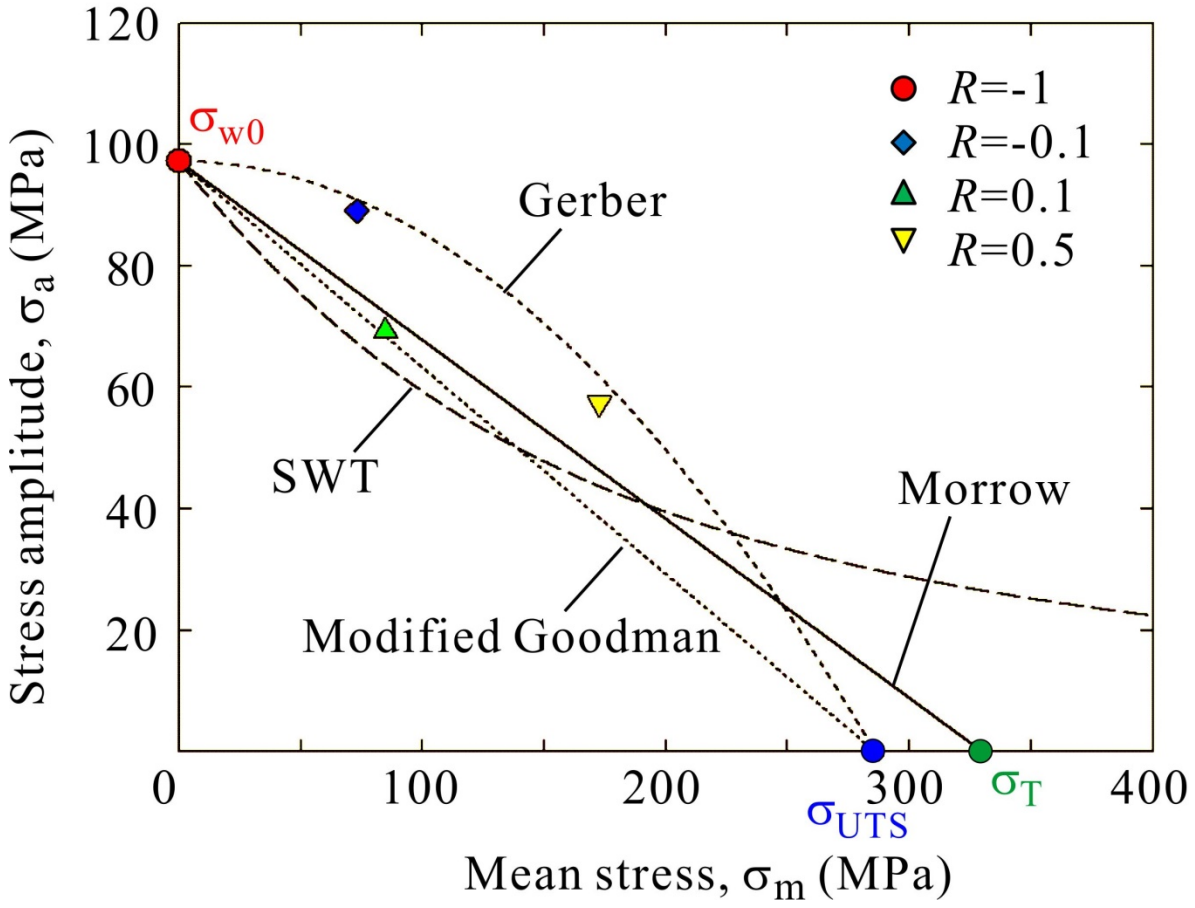

Figure 4. Fatigue limit diagram.

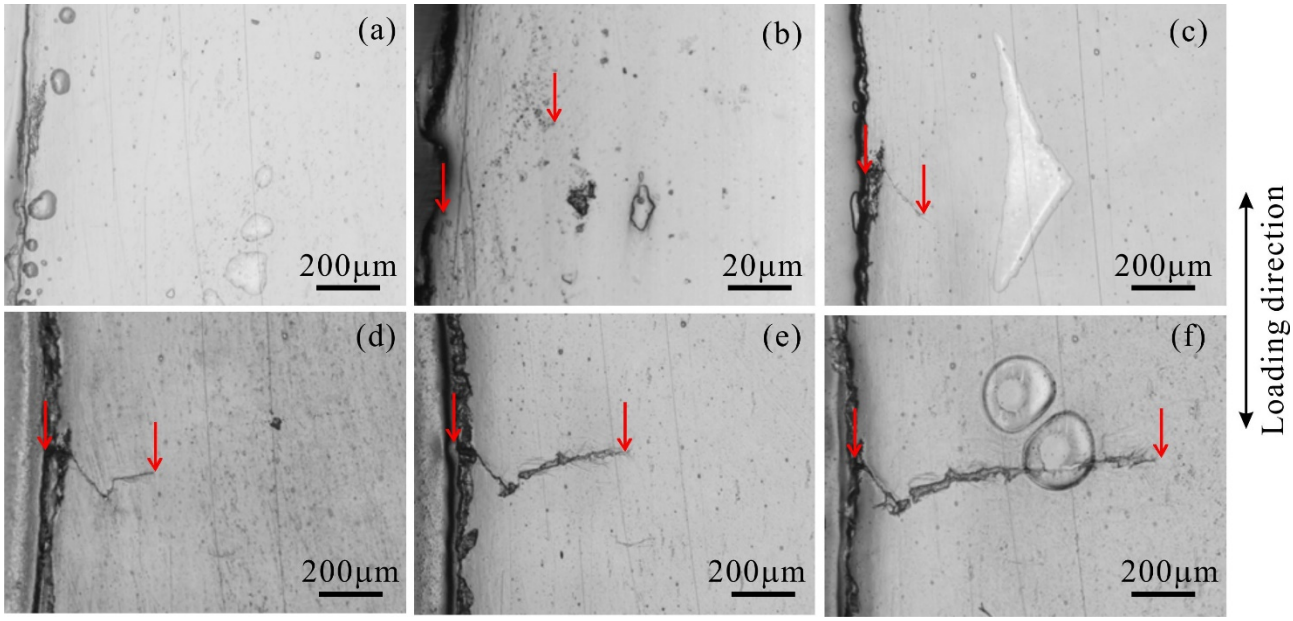

Figure.5. Propagation of the main crack at the surface at stress amplitude of 140 MPa under R =-1 and N_f=2.30×10^4 cycles determined by replicas at N= (a) 0, (b) 3.0×10^3, (c) 8.0×10^3, (d) 1.2×10^4, (e) 1.6×10^4, (f) 2.0×10^4 cycles, respectively.

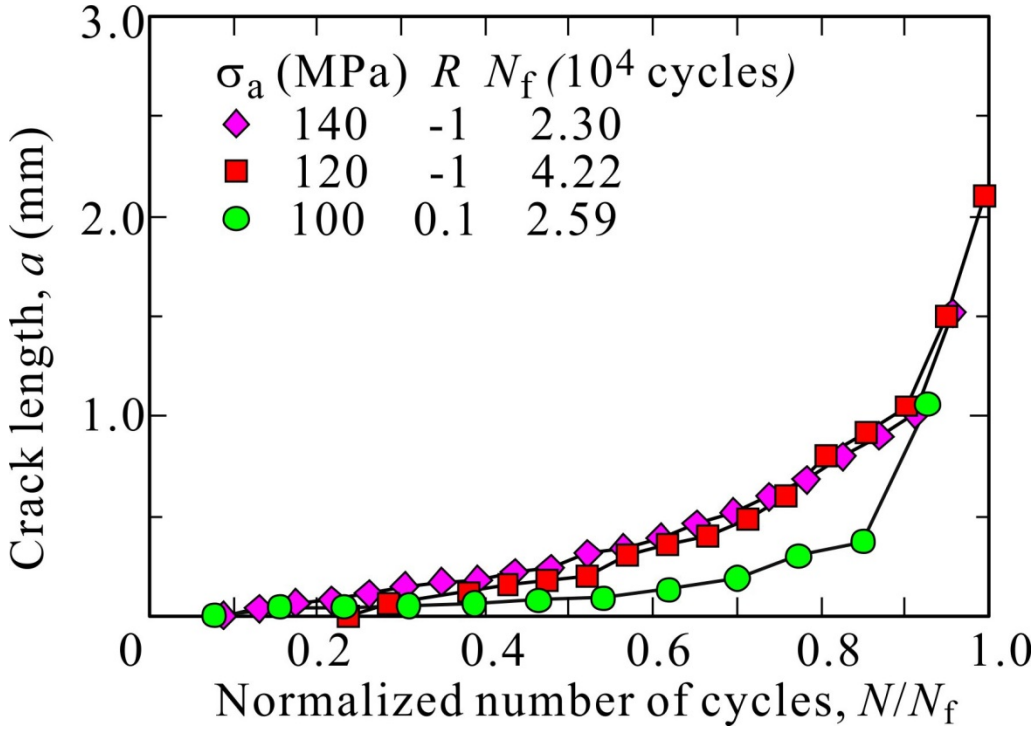

Figure 6. Relationship between crack length and normalized fatigue life.

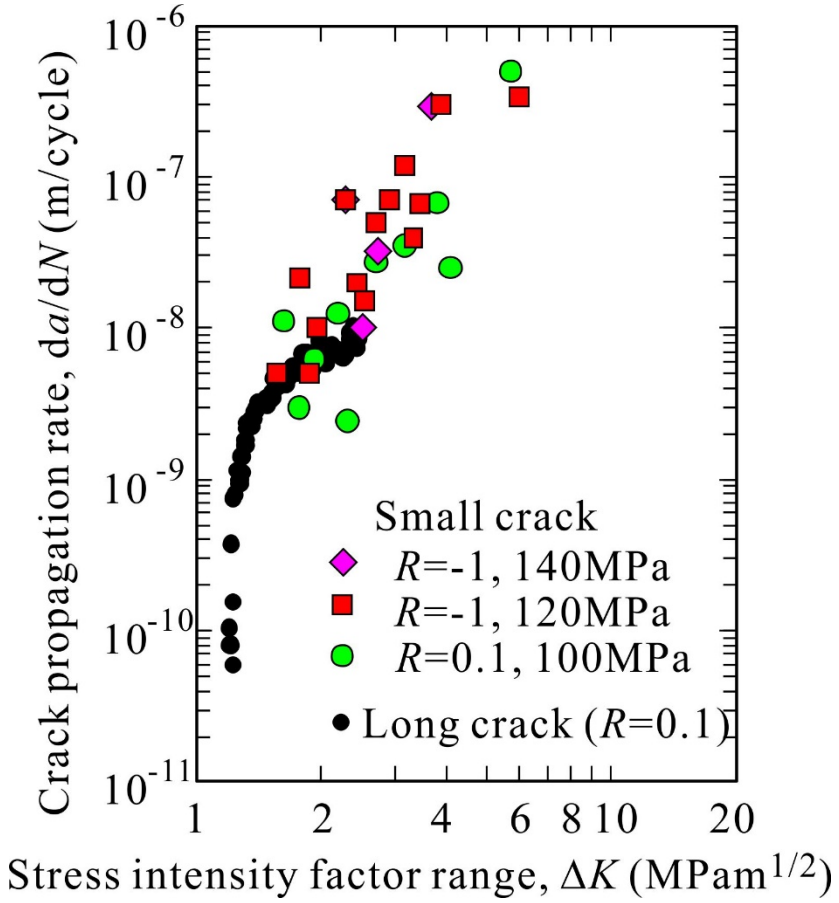

Figure 7. Crack growth behaviors of small cracks formed in smooth specimens.

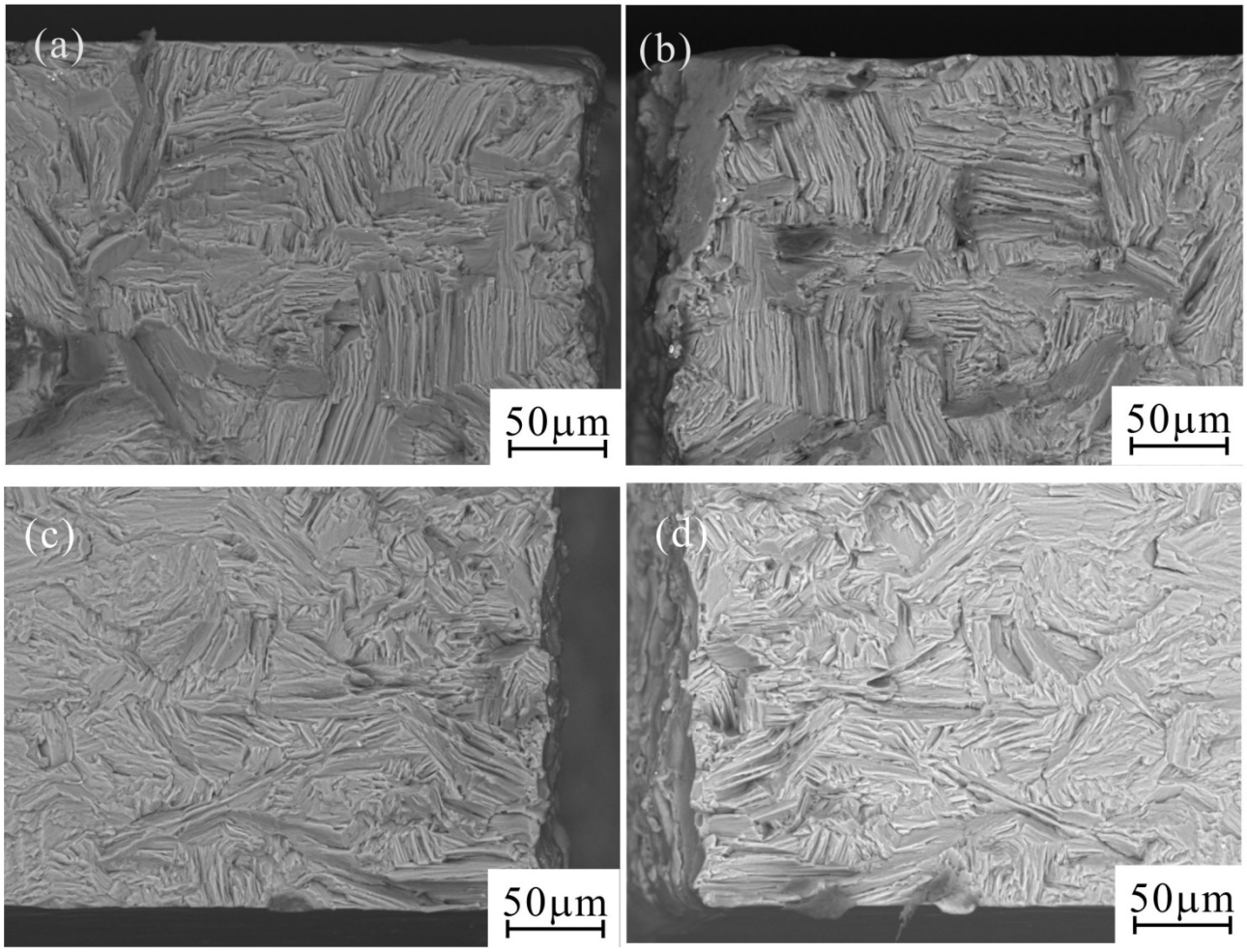

Figure 8. SEM micrographs of fracture surfaces, where (a), (b) σ_a = 120 MPa, R=-1, N_f = 4.21×10^4 cycles (c), (d) σ_a = 100 MPa, R=0.1, N_f = 2.59×10^4 cycles.

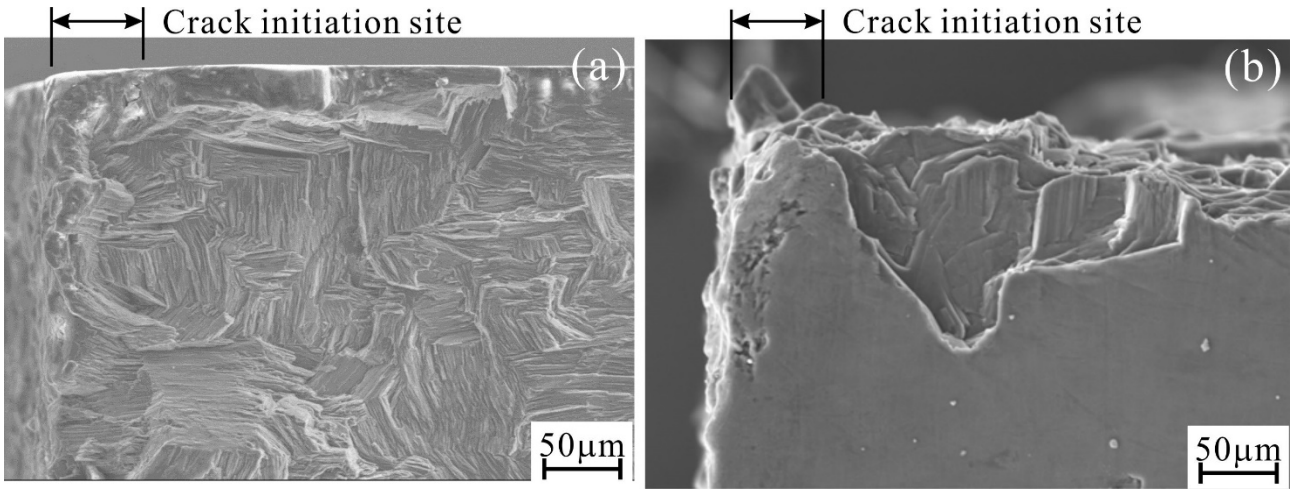

Figure 9. SEM micrograph showing an example of crack initiation site (R=-1, σ_a = 140 MPa, N_f = 2.30×10^4 cycles), where (a) fracture surface, (b) specimen surface.

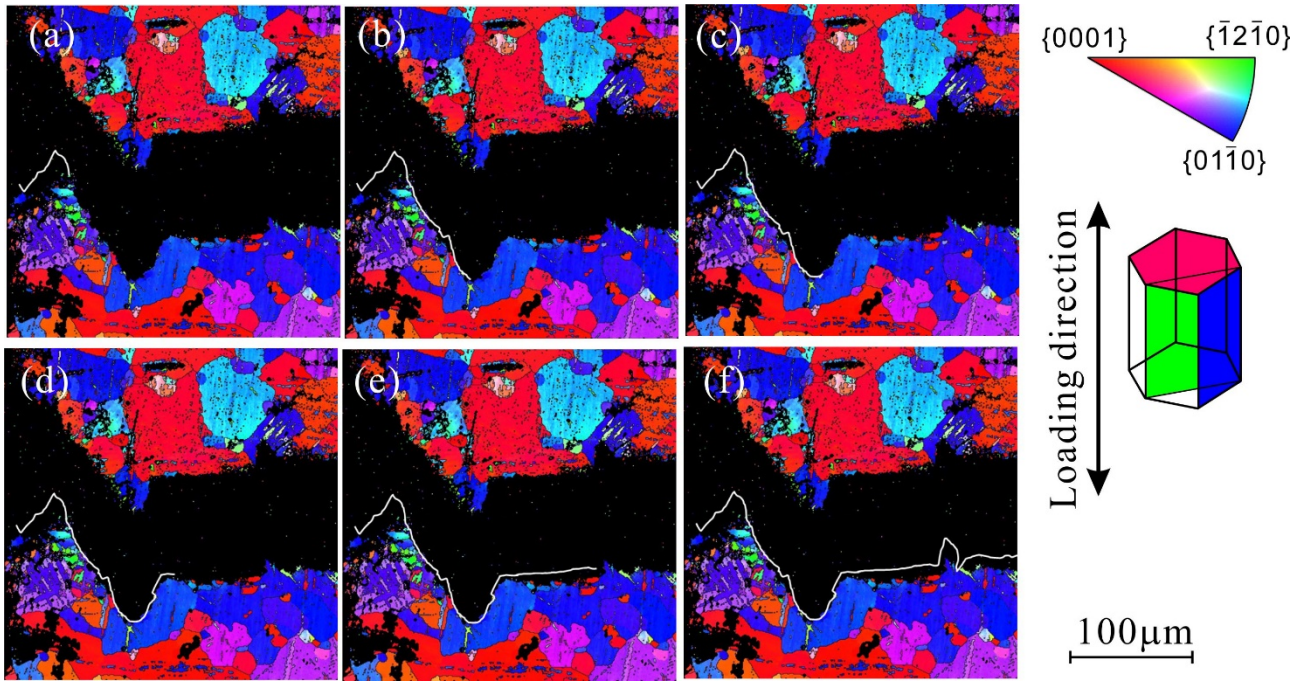

Figure 10. Inverse pole figure (IPF) map obtained by EBSD analysis failed at stress amplitude of 140 MPa under the stress ratio, *R*, of -1, at *N*= (a) 3.0×10^3, (b) 6.0×10^3, (c) 8.0×10^3, (d) 1.0×10^4, (e) 1.2×10^4, (f) 1.4×10^4 cycles, respectively, where white lines indicate the crack profile at the number of cycles.

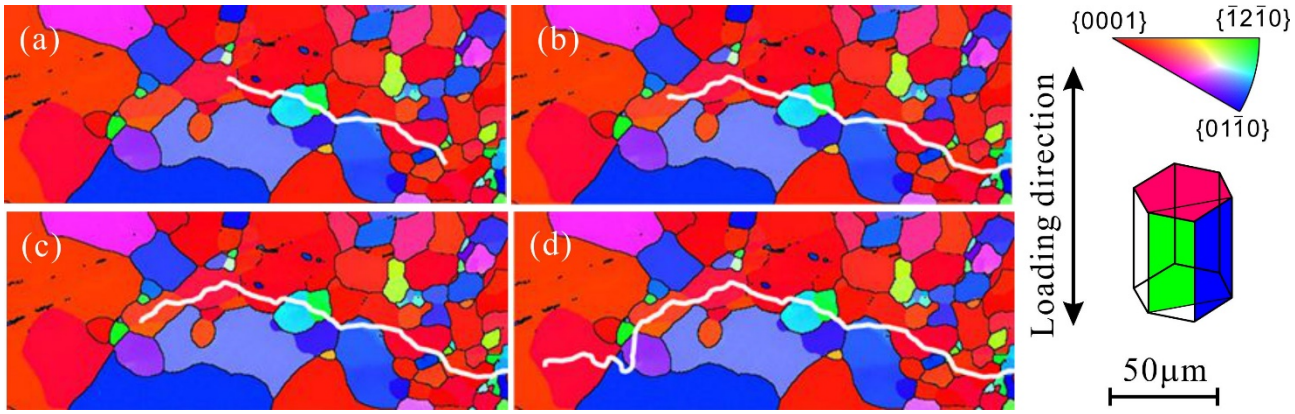

Figure 11. Inverse pole figure (IPF) map obtained by EBSD analysis of specimen fatigued at the stress amplitude of 140 MPa under the stress ratio, *R*, of -1, at *N*= (a) 1.0×10^3, (b) 2.0×10^3, (c) 3.0×10^3, (d) 4.0×10^3 cycles, respectively, where white lines indicate the crack profile at the number of cycles.

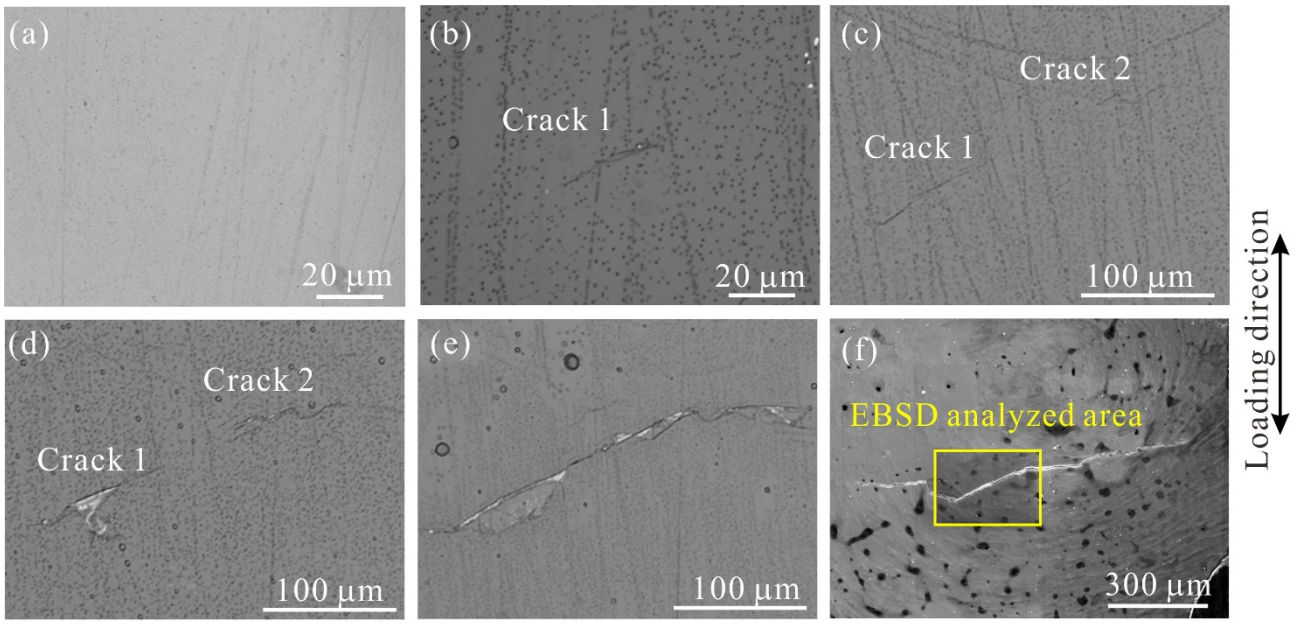

Figure 12. Crack initiation and propagation behaviors for a specimen fatigued under σ_a=120 MPa, R = -1, at N= (a) 0, (b) 2.0×10^3, (c) 4.0×10^3, (d) 1.2×10^4, (e) 2.0×10^4, (f) 6.0×10^4 cycles, respectively.

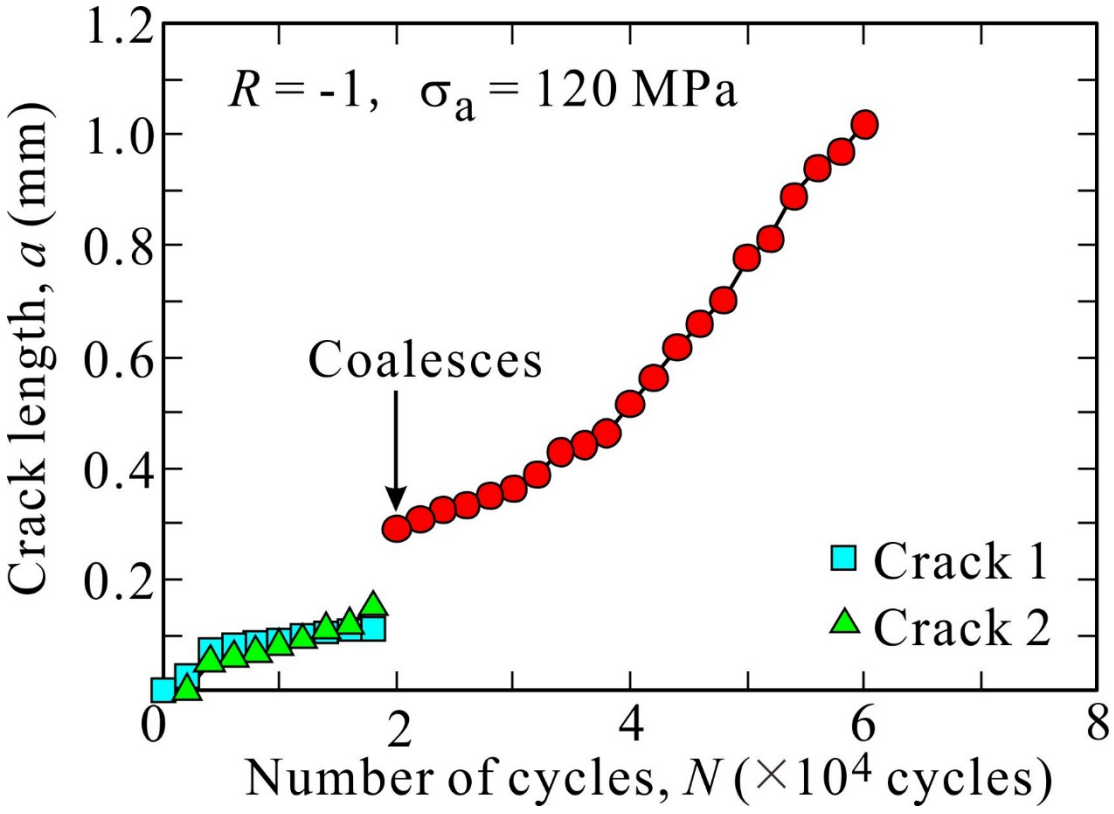

Figure 13. Crack growth curves.

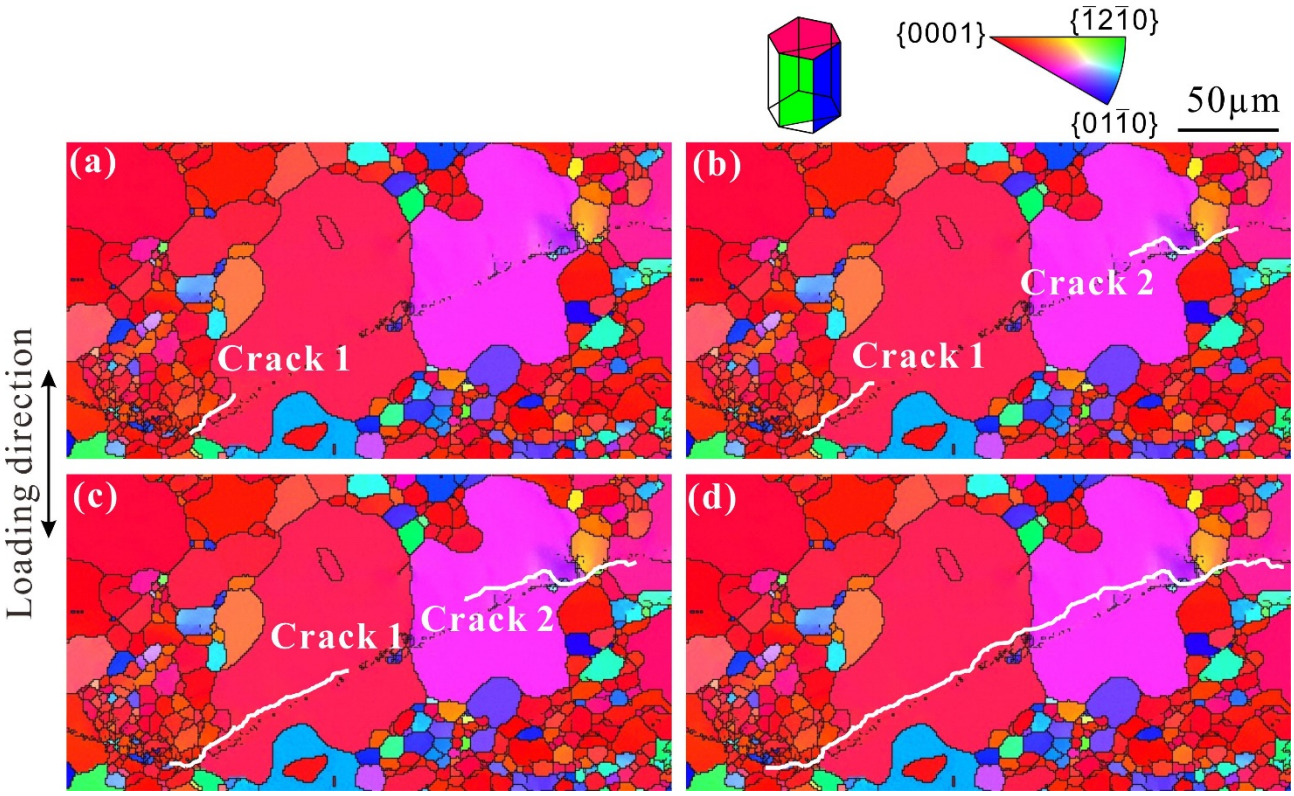

Figure 14. Orientation of grains around crack initiation site under σ_a=120 MPa, R = -1, at N= (a) 2.0×10^3, (b) 4.0×10^3, (c) 1.2×10^4, (d) 2.0×10^4 cycles, respectively, where white lines indicate the crack profile at the number of cycles.

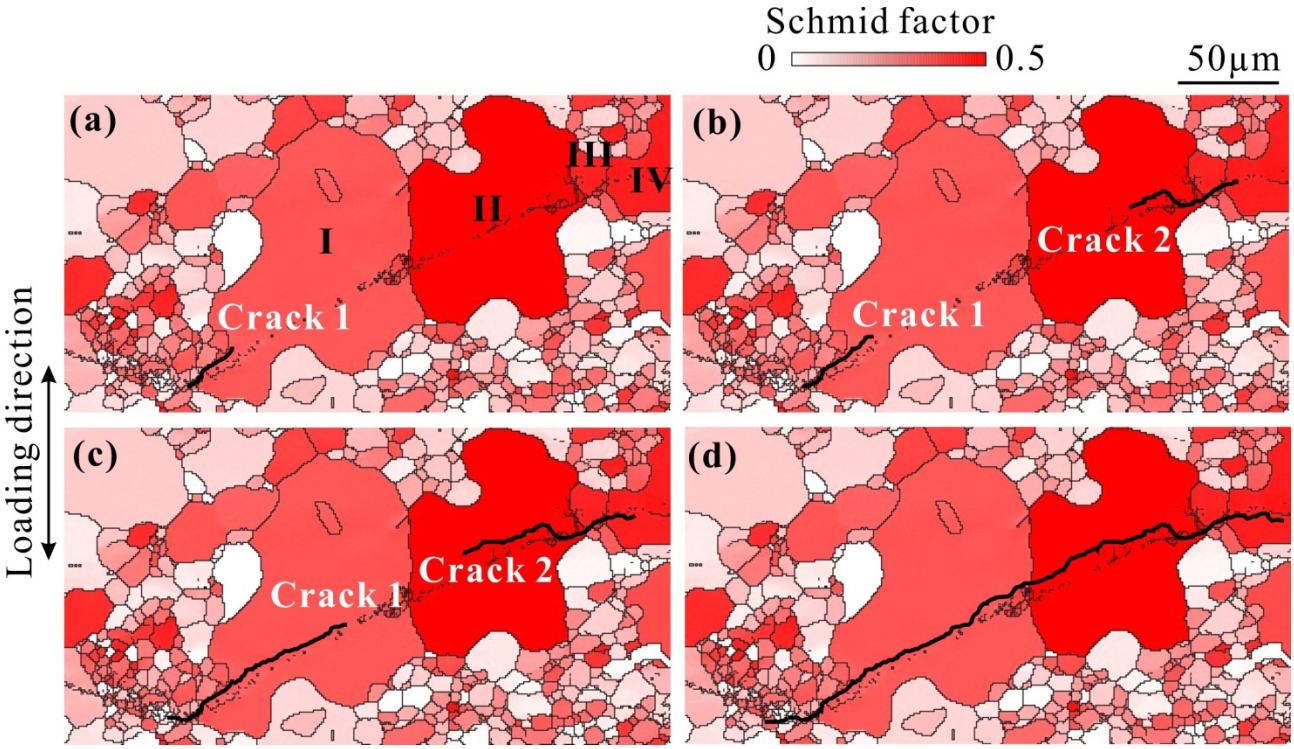

Figure 15. Schmid factor of basal slip system for grains around crack initiation site and crack profiles under σ_a=120 MPa, R = -1, at N= (a) 2.0×10^3, (b) 4.0×10^3, (c) 1.2×10^4, (d) 2.0×10^4 cycles, respectively, where black lines indicate the crack profile at the number of cycles.